A^0Z^0 associated production at the CERN Large Hadron Collider in the minimal supersymmetric standard model

Yin Jun,[2] Ma Wen-Gan,[1,2] Zhang Ren-You,[2] and Hou Hong-Sheng[2]
[1]*CCAST (World Laboratory), P.O. Box 8730, Beijing 100080, China*
[2]*Department of Modern Physics, University of Science and Technology of China (USTC), Hefei, Anhui 230027, China*
(Received 25 July 2002; published 19 November 2002)

We investigate in detail the A^0Z^0 associated production process $pp \to A^0Z^0 + X$ within the framework of the minimal supersymmetric standard model (MSSM) at the CERN Large Hadron Collider (LHC), considering contributions from both the Drell-Yan and gluon fusion subprocesses. We focus on the deviations from the general two-Higgs-doublet model (2HDM) arising in the MSSM. We also discuss the contributions of the two A^0Z^0 associated production subprocesses in the MSSM at the CERN LHC and analyze the dependences of the total cross section on neutral CP-odd Higgs boson mass m_A and $\tan\beta$ in the MSUGRA scenario. We find that the contribution from the loop mediated gluon fusion subprocess can be competitive with that from the Drell-Yan subprocess in some parameter space.

DOI: 10.1103/PhysRevD.66.095008 PACS number(s): 12.60.Jv, 12.15.Lk, 12.60.Fr, 14.80.Cp

I. INTRODUCTION

The minimal standard model (MSM) [1,2] has been proved by all precise experimental data so that the MSM is a very successful model of particle physics. But until now the symmetry breaking structure of the electroweak interactions has not yet been directly explored experimentally. So the exploration of the SM Higgs boson is a major goal of present and future colliders. As we know, any enlargement of the Higgs sector beyond the single $SU(2)_L$ Higgs doublet of the MSM necessarily introduces other neutral Higgs bosons and charged Higgs bosons. Like the general two-Higgs-doublet model (2HDM), the minimal supersymmetric standard model (MSSM) [3,4] requires the introduction of two Higgs doublets in order to preserve supersymmetry. These two Higgs doublets predict some more elementary Higgs bosons: one CP-even neutral Higgs boson (H^0), one CP-odd neutral Higgs boson (A^0), and two charged Higgs bosons ($H^\pm$), which are absent in the MSM. Any experimental discovery of these non-SM-like Higgs bosons will be direct verification of these extended versions of the Higgs sector. Therefore, the study of various production mechanisms of the non-SM-like Higgs bosons at present and future colliders is well motivated.

Searching for non-SM-like Higgs bosons and studying their properties at future multi-TeV hadron colliders, such as the CERN Large Hadron Collider (LHC), are possible, as expected by supersymmetric (SUSY) theory [3,5]. The gluon fusion mechanism $gg \to \phi(\phi = h^0, H^0, A^0)$ provides the dominant production mechanism of neutral Higgs bosons at the LHC in the entire relevant mass range up to about 1 TeV for small and moderate values of $\tan\beta$ in the MSSM [6]. The heavy neutral Higgs boson can be also produced in pairs (A^0A^0, A^0h^0, A^0H^0) at the LHC, if it is kinematically allowed [7]. Studying the process of a heavy charged Higgs boson associated with the W boson is another attractive way to search for $H^\pm$ bosons, because the $W^\pm$ boson's leptonic decay may be used as a spectacular trigger. The calculations of the heavy $H^\pm$ production associated with the $W^\mp$ boson at a future electron-positron collider can be found in Refs. [8–12]. The complete calculations of the $H^\pm W^\mp$ associated production at hadron colliders both in the 2HDM and MSSM are given in Refs. [13–17]. Analogously, A^0Z^0 associated production would also be an efficient way to search for the heavy neutral CP-odd Higgs boson A^0. Although the A^0 boson can be produced in pairs at future colliders [7,18], the A^0Z^0 associated production will be the kinematically favorite mechanism to produce the A^0 Higgs boson for the heavy A^0 Higgs boson. And again the leptonic decay of Z^0 may benefit from triggering the Z^0A^0 associated production events. The calculations of the Z^0A^0 associated production at a electron-positron collider were presented in Refs. [19,20], at a muon collider in Ref. [21], and at a photon collider in Ref. [22], respectively, and Chung Kao gave the calculation of A^0Z^0 associated production via gg fusion including only quark loop diagrams at the SSC [23].

In this paper we concentrate on studying the A^0Z^0 associated production at the LHC in the MSSM, considering both subprocesses $q\bar{q} \to A^0Z^0$ and $gg \to A^0Z^0$. In the calculation of the loop mediated process $pp \to gg \to A^0Z^0$, we compare and discuss the cross sections in the general 2HDM and MSSM. In Sec. II, we present the calculation of the processes $pp \to q\bar{q} \to A^0Z^0$ and $pp \to gg \to A^0Z^0$. Numerical results and discussion are given in Sec. III. There we use the MSSM parameters constrained within the minimal supergravity (MSUGRA) scenario [24]. Finally, a short summary is given.

II. CROSS SECTION CALCULATION

In our calculation we use the 't Hooft–Feynman gauge and adopt the dimension regularization scheme in the general 2HDM and the dimensional reduction (DR) scheme [25] in the MSSM. In the loop diagram calculation we adopted the definitions of one-loop integral functions in Ref. [26]. The numerical calculation of the vector and tensor loop integral functions can be traced back to scalar loop integrals as shown in Ref. [27]. The Feynman diagrams and relevant am-

 ©2002 The American Physical Society

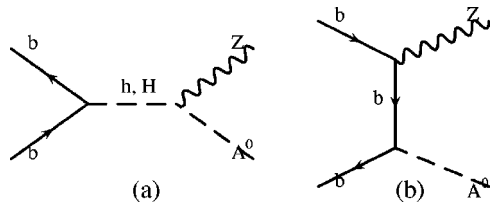

FIG. 1. The relevant Feynman diagrams for the subprocess $b\bar{b} \to A^0Z^0$ in the MSSM at the tree level: (a) *s*-channel diagrams. (b) *u*- and *t*-channel diagrams. Note that (b) includes the diagram created by exchanging two final states.

plitudes are created by the FEYNARTS package automatically [28]. The numerical calculations of the loop integrals are implemented by using MATHEMATICA programs.

A. Calculation of the subprocess $q\bar{q} \to A^0Z^0 + X$

We denote the A^0Z^0 associated production via the Drell-Yan subprocess as

$$q(p_1) + \bar{q}(p_2) \to Z^0(k_1) + A^0(k_2). \tag{2.1}$$

As a result of the feature of the Yukawa coupling that the coupling strength between quarks and Higgs bosons is in proportion to the corresponding quark mass, the cross sections of subprocesses $q\bar{q} \to A^0Z^0 (q = u,d,s,c)$ should be much smaller than those of subprocesses $t\bar{t}(b\bar{b}) \to A^0Z^0$. Considering the fact that the luminosity of the top (antitop) quark is much lower than that of bottom (antibottom) quark from a proton, we conclude that the cross section of the process $pp \to q\bar{q} \to A^0Z^0 + X$ is approximately equal to the cross section of $pp \to b\bar{b} \to A^0Z^0 + X$. Therefore, in this paper we consider only the contributions from the $pp \to b\bar{b} \to A^0Z^0 + X$ process.

The Feynman diagrams of the subprocess $b\bar{b} \to A^0Z^0$ at lowest order are depicted in Fig. 1. The differential cross section of the subprocess $b\bar{b} \to A^0Z^0$ can be expressed as

$$d\hat{\sigma}_{b\bar{b}} = dP_{2f} \frac{1}{12} \sum_{spin} |A_{(a)}(\hat{s},\hat{t},\hat{u}) + A_{(b)}(\hat{s},\hat{t},\hat{u})|^2, \tag{2.2}$$

where the summation is taken over the spins of the initial and final states, and dP_{2f} denotes the two-particle phase space element. The factor of 1/12 in the above equation comes from averaging over the spins and colors of the incoming partons. The matrix element $A_{(a)}$ represents the amplitude of the $h^0(H^0)$ exchanging *s*-channel diagrams [shown in Fig. 1(a)], and $A_{(b)}$ corresponds to the amplitude of the *u*- and *t*-channel diagrams [shown in Fig. 1(b)]. The Mandelstam kinematical variables are defined as

$$\hat{s} = (p_1 + p_2)^2, \quad \hat{t} = (p_1 - k_1)^2, \quad \hat{u} = (p_1 - k_2)^2. \tag{2.3}$$

By using the relevant Feynman rules, we obtain the explicit expressions of these amplitudes:

$$\begin{aligned} A_{(a)}(\hat{s},\hat{t},\hat{u}) = & -\frac{(4\pi\alpha)m_b}{4s_W^2 c_W^2} \cos(\beta-\alpha) \frac{\sin\alpha}{\cos\beta} \epsilon^{\mu}(k_1) \\ & \times [\bar{v}(p_2) u(p_1)] \frac{(k_1+p_1+p_2)^{\mu}}{\hat{s} - m_h^2 + m_h \Gamma_h i} \\ & - \frac{(4\pi\alpha_s)m_b}{4s_w^2 c_W^2} \sin(\beta-\alpha) \frac{\cos\alpha}{\cos\beta} \epsilon^{\mu}(k_1) \\ & \times [\bar{v}(p_2) u(p_1)] \frac{(k_1+p_1+p_2)^{\mu}}{\hat{s} - m_H^2 + m_H \Gamma_H i}, \end{aligned}$$

$$\begin{aligned} A_{(b)}(\hat{s},\hat{t},\hat{u}) = & -\frac{(4\pi\alpha)m_b}{2m_W s_W^2 c_W} \tan\beta \epsilon^{\mu}(k_1) \frac{1}{\hat{t} - m_b^2} \Bigg[\bar{v}(p_2) \gamma^5 \\ & \times (m_b - \not{k}_1 + \not{p}_1) \gamma^{\mu} \left(\frac{s_W^2}{3} - \frac{P_L}{2} \right) u(p_1) \Bigg] \\ & - \frac{(4\pi\alpha)m_b}{2m_W s_W^2 c_W} \tan\beta \epsilon^{\mu}(k_1) \frac{1}{\hat{u} - m_b^2} \Bigg[\bar{v}(p_2) \gamma^5 \\ & \times (m_b + \not{k}_1 - \not{p}_2) \gamma^{\mu} \left(\frac{s_W^2}{3} - \frac{P_L}{2} \right) u(p_1) \Bigg], \end{aligned} \tag{2.4}$$

where m_b and m_W represent the masses of bottom quark and *W* boson, respectively.

B. Calculation of the subprocess $gg \to A^0Z^0 + X$

We denote the A^0Z^0 associated production process via gluon fusions as

$$g(p_1,\alpha) + g(p_2,\beta) \to Z^0(k_1) + A^0(k_2), \tag{2.5}$$

where α, β are the color indices of initial gluons. As the subprocess $gg \to Z^0A^0$ is loop induced, the one-loop order calculation can be simply carried out by summing all unrenormalized reducible and irreducible one-loop diagrams and the results will be finite and gauge invariant. We denote σ_{gg}^{2HDM} and σ_{gg}^{MSSM} as the cross sections in the framework of the general 2HDM and MSSM, respectively. The former is contributed by the Feynman diagrams involving only the quark loop diagrams (shown in Fig. 2) and the latter involves the contributions of both the quark and squark loop diagrams (shown in Figs. 2 and 3). The possible corresponding Feynman diagrams created by exchanging the initial gluons or two final states should also be included in Figs. 2 and 3 and involved in our calculation.

We can see that each Feynman diagram in Figs. 2 and 3 contains one interacting vertex between (s)quarks and a Higgs boson. As a result of the feature of the Yukawa coupling as we mentioned above, we can consider only the diagrams which involve the third generation (s)quark in the calculation of the subprocess $gg \to A^0Z^0$. The cross sections of the subprocess $gg \to A^0Z^0$ in the general 2HDM and MSSM can be expressed, respectively, as

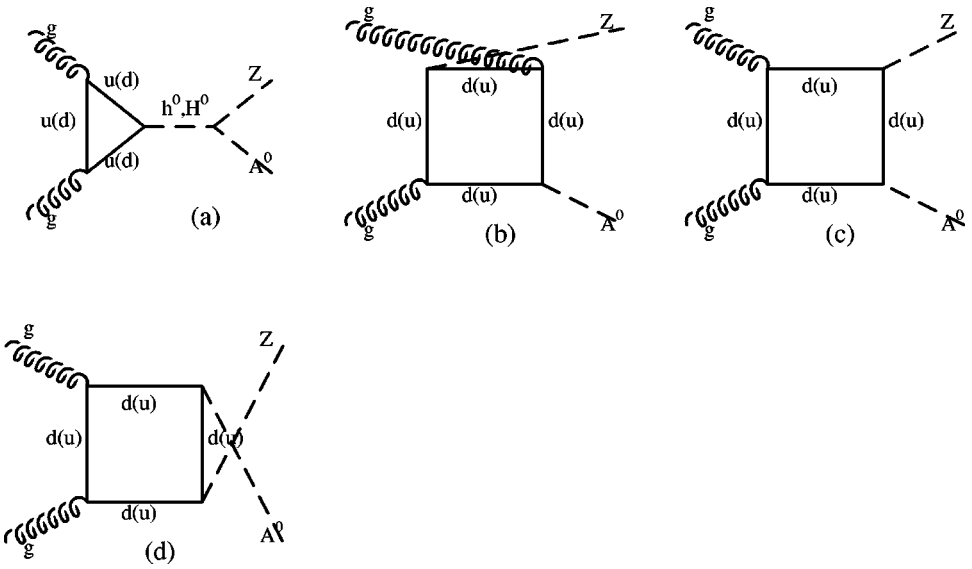

FIG. 2. The relevant Feynman diagrams for the subprocess $gg \rightarrow Z^0A^0$ at the one-loop level (including only the quark loop diagrams).

$$d\hat{\sigma}_{gg}^{2HDM} = dP_{2f}\frac{1}{256}\sum |A_{(a)}^{(2)}(\hat{s},\hat{t},\hat{u}) + A_{(b)}^{(2)}(\hat{s},\hat{t},\hat{u}) + A_{(c)}^{(2)}(\hat{s},\hat{t},\hat{u})|^2,$$

$$d\hat{\sigma}_{gg}^{MSSM} = dP_{2f}\frac{1}{256}\sum |A_{(a)}^{(2)}(\hat{s},\hat{t},\hat{u}) + A_{(b)}^{(2)}(\hat{s},\hat{t},\hat{u}) + A_{(c)}^{(2)}(\hat{s},\hat{t},\hat{u}) + A_{(a)}^{(3)}(\hat{s},\hat{t},\hat{u}) + A_{(b)}^{(3)}(\hat{s},\hat{t},\hat{u}) + \cdots + A_{(g)}^{(3)}(\hat{s},\hat{t},\hat{u})|^2, \quad (2.6)$$

where the summation is taken over the spins and colors of the initial and final states, and dP_{2f} denotes the two-particle phase space element. $A_{(j)}^{(i)}$ (i=2,3; j=a,b,c...) represents the amplitude of the sub-figures of Fig. 2(a), Fig. 2(b)... Fig. 3(a), Fig. 3(b)...respectively. The factor of 1/256 results from averaging over the spins and colors of the incoming partons.

C. Cross section of the $pp \rightarrow A^0Z^0 + X$ process at the LHC

With the cross sections of the related subprocesses, the cross section of the parent process $pp \rightarrow A^0Z^0 + X$ at the proton-proton collider LHC can be obtained by doing the following integration:

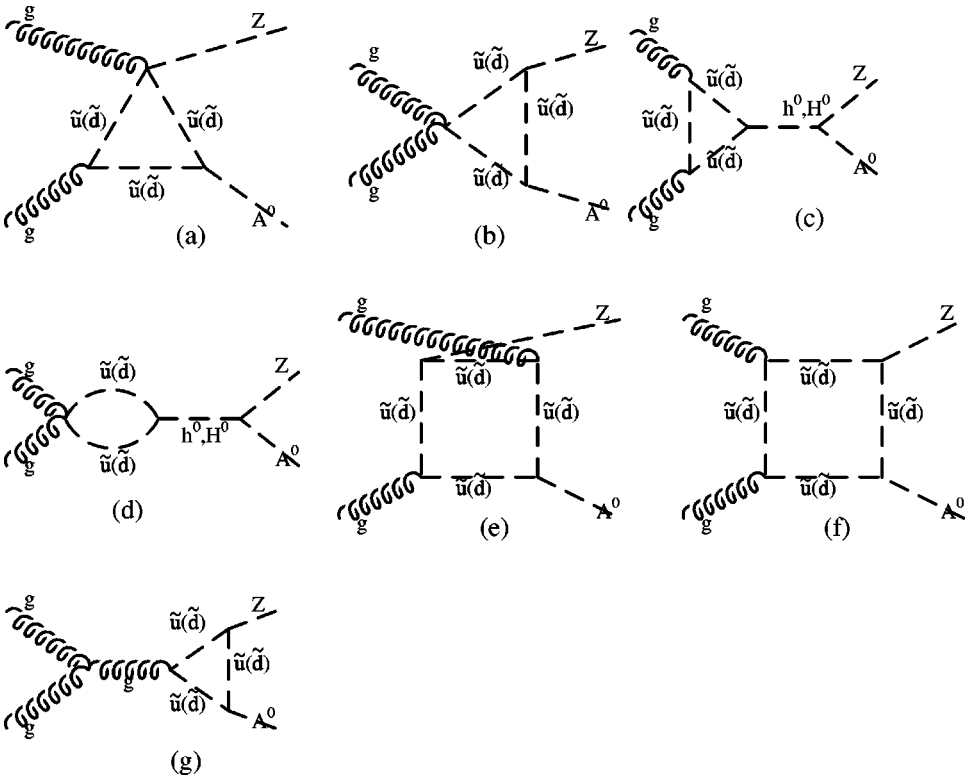

FIG. 3. The relevant Feynman diagrams for the subprocess $gg \rightarrow A^0Z^0$ at the one-loop level (including only the scalar quark loop diagrams).

$$\sigma_{ij}=\int_{(m_Z+m_A)^2/s}^{1} d\tau \frac{d\mathcal{L}_{ij}}{d\tau}\hat{\sigma}_{ij}(\hat{s}=\tau s), \tag{2.7}$$

where

$$\frac{d\mathcal{L}_{ij}}{d\tau}=\frac{1}{1+\delta_{ij}}\int_{\tau}^{1}\frac{dx_1}{x_1}\left\{\left[f_{i/p}(i,x_1,Q^2)f_{j/p}\left(j,\frac{\tau}{x_1},Q^2\right)\right]+\left[f_{j/p}(j,x_1,Q^2)f_{i/p}\left(i,\frac{\tau}{x_1},Q^2\right)\right]\right\}. \tag{2.8}$$

In Eq. (2.7), $\sqrt{s}$ and $\sqrt{\hat{s}}$ are the colliding proton-proton and parton-parton c.m. system (c.m.s.) energies, respectively. The notation σ_{ij} represents the cross section of the parent process $pp\to ij\to A^0Z^0+X$. Here $d\mathcal{L}_{ij}/d\tau$ is the luminosity of incoming partons where i, j can be b, $\bar{b}$ and g, $\tau=x_1x_2$. Also, m_Z and m_A represent the masses of the Z^0 boson and A^0 Higgs boson. The definitions of x_1 and x_2 can be found in Ref. [29]. In our calculation, we adopt the CTEQ5 parton distribution function [30] and take the factorization scale Q to be $\sqrt{\hat{s}}$. Equation (2.7) can be rewritten as

$$\sigma_{ij}=\int_{m_Z+m_A}^{\sqrt{s}} d\sqrt{\hat{s}}\hat{\sigma}_{ij}(\hat{s})H_{ij}(\hat{s}), \tag{2.9}$$

where

$$H_{ij}(\hat{s})=\frac{1}{1+\delta_{ij}}\int_{\hat{s}/s}^{1}\frac{2dx_1\sqrt{\hat{s}}}{x_1 s}\times\left\{\left[f_{i/p}(i,x_1,Q^2)f_{j/p}\left(j,\frac{\hat{s}}{x_1 s},Q^2\right)\right]+(i\leftrightarrow j)\right\}. \tag{2.10}$$

When $ij=gg$, σ_{gg}^{2HDM} represents the cross section of the parent process $pp\to gg\to A^0Z^0+X$ contributed only by the quark loop diagrams shown in Fig. 2, while σ_{gg}^{MSSM} represents the cross section contributed by both the quark and squark loop diagrams shown in Figs. 2 and 3. In the next section we shall take different input data sets to demonstrate the production rates of the parent process $pp\to A^0Z^0+X$. The numerical results of σ_{gg}^{2HDM} and σ_{gg}^{MSSM} would show the importance of squark loop diagrams. The total cross section of $pp\to A^0Z^0+X$ at the proton-proton collider should be the summation of $\sigma_{b\bar{b}}$ and σ_{gg}. Quantitatively comparing $\sigma_{b\bar{b}}$ with σ_{gg} will help us to know in which part of the parameter space the contribution of the gluon-gluon fusion process is dominant.

III. NUMERICAL RESULT AND DISCUSSION

A. Input parameters

In the numerical calculation, we take the SM parameters as $m_t=174.3$ GeV, $m_b=4.2$ GeV, $m_Z=91.187$ GeV, and $\Gamma_Z=2.49$ GeV [31] and take the supersymmetric parameters as being constrained within the MSUGRA scenario [24]. In this scenario, only five sypersymmetric parameters should be input: namely, $M_{1/2}$, M_0, A_0, the sign of μ, and $\tan\beta$, where $M_{1/2}$, M_0, and A_0 are the universal gaugino mass, scalar mass at the ground unified theory (GUT) scale, and the trilinear soft breaking parameter in the superpotential terms, respectively. In this work, we take $M_{1/2}=120$ GeV, $A_0=300$ GeV, and $\mu>0$. Here M_0 is obtained quantitatively from the input m_A value. All other MSSM parameters are determined in the MSUGRA scenario by using the program package ISAJET 7.44. In this program, the renormalization group equations (RGEs) [32] run from the weak scale m_Z up to the GUT scale, taking all thresholds into account in order to get the low energy scenario from the MSUGRA. It uses two-loop RGEs only for the gauge couplings and one-loop RGEs for the other supersymmetric parameters. The GUT scale boundary conditions are imposed and the RGEs are run back to m_Z, again taking the threshold into account.

Here we give some comments about the choice of the decay width values of CP-even neutral Higgs bosons h^0 and H^0. We know that some of the Feynman diagrams (shown in Figs. 1–3) have s-channel h^0 and H^0 propagators, which have analytical expressions, respectively, as

$$\frac{1}{\hat{s}-m_h^2+im_h\Gamma_h}=\frac{\hat{s}-im_h^2-m_h\Gamma_h}{(\hat{s}-m_h^2)^2+m_h^2\Gamma_h^2}, \tag{3.1}$$

$$\frac{1}{\hat{s}-m_H^2+im_H\Gamma_H}=\frac{\hat{s}-m_H^2-im_H\Gamma_H}{(\hat{s}-m_H^2)^2+m_H^2\Gamma_H^2}. \tag{3.2}$$

It is clear that the cross sections of the subprocess should related to the decay widths of h^0 and H^0. In this work the input parameter m_A is taken in the range of 200–650 GeV. Then we have the following constraints in this parameter space:

$$m_H\approx m_A, \quad m_h<150 \text{ GeV}, \tag{3.3}$$

and by using the package HDECAY [33] in the MSSM, we find

$$\Gamma_H,\ \Gamma_h<10 \text{ GeV}. \tag{3.4}$$

Because $\sqrt{\hat{s}}\geqslant m_A+m_Z$, we get $(\hat{s}-m_H^2)^2\gg m_H^2\Gamma_H^2$. The propagator of H^0 boson can be expressed approximately as

$$\frac{\hat{s}-m_H^2-im_H\Gamma_H}{(\hat{s}-m_H^2)^2+m_H^2\Gamma_H^2}\approx\frac{1}{(\hat{s}-m_H^2)}. \tag{3.5}$$

It is obvious that the bigger the $\sqrt{\hat{s}}$ is, the less sensitive is the cross section to the decay widths of neutral Higgs bosons H^0 and h^0. Therefore, we choose $\Gamma_H=\Gamma_h=10$ GeV in our numerical calculations. Actually, our final numerical result of the cross section of the process $pp\to A^0Z^0+X$ at the LHC shows also that it is not sensitive to the choice of these two decay widths.

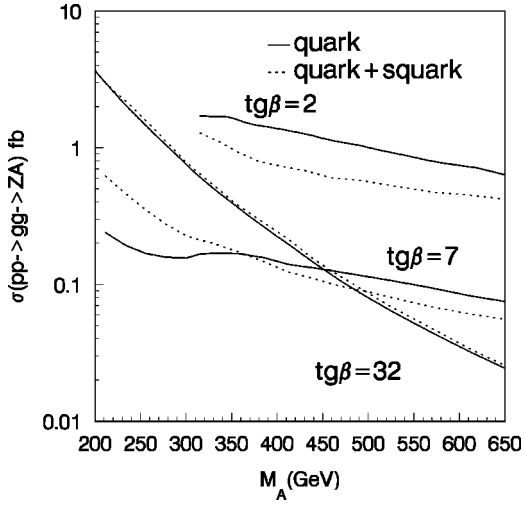

FIG. 4. The cross sections σ_{gg}^{2HDM} and σ_{gg}^{MSSM} of the process $pp \to gg \to A^0Z^0+X$, as functions of the mass of Higgs boson A^0. The input parameter $\tan\beta$ is taken as 2, 7, and 32, respectively.

B. Discussion and analysis

Figures 4, 5, and 6 show the cross sections (or differential cross sections) of the process $pp \to gg \to A^0Z^0+X$ at the LHC as the functions of the CP-odd Higgs boson A^0 mass, the ratio of the vacuum expectation values $\tan\beta$, and the transverse momentum p_T, respectively. The curves of the cross sections (or differential cross sections) involving the contributions from quark loop diagrams (in the general 2HDM) and quark+squark loop diagrams (in the MSSM) are depicted separately in these figures for comparison of the cross sections in these two models. And in these three figures the solid lines are for σ_{gg}^{2HDM} (or $d\sigma_{gg}^{2HDM}/dp_T$), and the dotted lines are for σ_{gg}^{MSSM} (or $d\sigma_{gg}^{MSSM}/dp_T$).

Figure 4 shows the relationship between the cross section of the parent process $pp \to gg \to A^0Z^0+X$ and m_A with colliding energy $\sqrt{s}=14$ TeV. The input MSUGRA parameters are set to be the typical values mentioned in the last subsection (i.e., $M_{1/2}=120$ GeV, $A_0=300$ GeV, and $\mu>0$; M_0 is obtained quantitatively from the m_A value) and $\tan\beta=2,7$, and 32, respectively. From this figure, we find that in some parameter space the scalar quark contributions can enhance the cross section obviously, that is to say, $\sigma_{gg}^{MSSM} > \sigma_{gg}^{2HDM}$, while in other regions, we have $\sigma_{gg}^{MSSM} < \sigma_{gg}^{2HDM}$. The figure shows that when we have small and moderate $\tan\beta$ values, the scalar quark loop contribution to the A^0Z^0 associated production at the LHC is most obvious. We shall also see later from Fig. 7 that when $\tan\beta$ has a small or moderate value, the contributions from the gluon fusion subprocess are dominant. Therefore, it is possible to use the experimental measurement of the A^0Z^0 associated production at the LHC

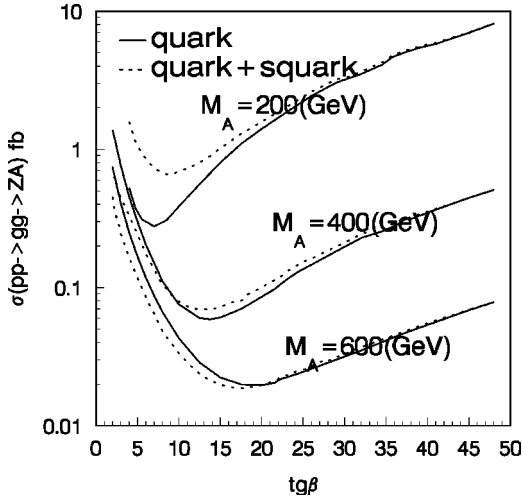

FIG. 5. The cross sections σ_{gg}^{2HDM} and σ_{gg}^{MSSM} of the process $pp \to gg \to A^0Z^0+X$, as functions of $\tan\beta$. The mass of the Higgs boson A^0 is taken as 200 GeV, 400 GeV, and 600 GeV, respectively.

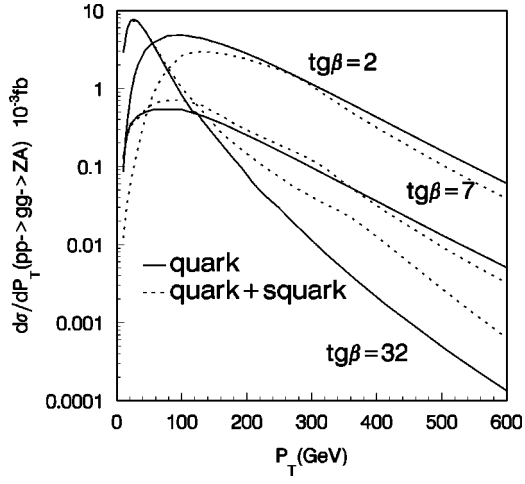

FIG. 6. The differential cross sections $d\sigma_{gg}^{2HDM}/dp_T$ and $d\sigma_{gg}^{MSSM}/dp_T$ of the process $pp \to gg \to A^0Z^0+X$, as functions of the transverse momentum p_T in the MSUGRA scenario at the LHC with $\sqrt{s}=14$ TeV, $m_A=350$ GeV, and the pseudorapidity being in the range of $|\eta|<2$. The ratio of the vacuum expectation values $\tan\beta$ is taken as 2, 7, and 32, respectively.

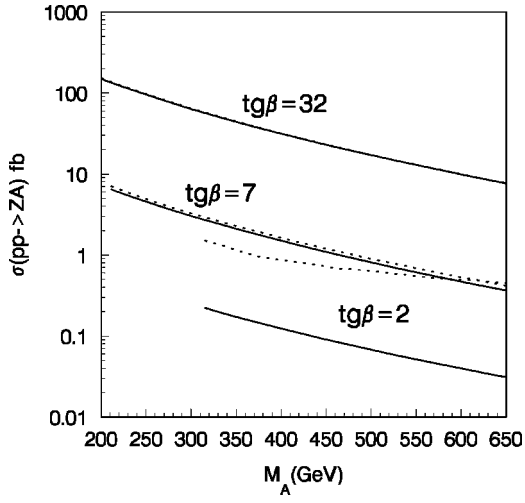

FIG. 7. The cross sections $\sigma^{(DY)}$ and $\sigma^{(T)}$ of the process $pp \to A^0Z^0+X$ as functions of the mass of the Higgs boson A^0. The ratio of the vacuum expectation values $\tan\beta$ is taken as 2, 7, and 32, respectively.

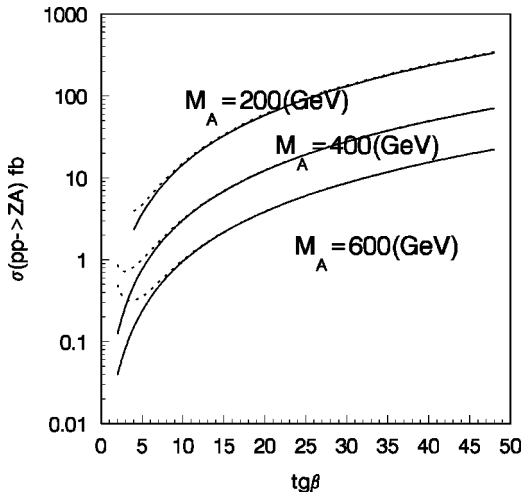

FIG. 8. The cross sections $\sigma^{(DY)}$ and $\sigma^{(T)}$ of the process $pp \rightarrow A^0Z^0+X$ as functions of $\tan\beta$. The mass of the Higgs boson A^0 is taken as 200 GeV, 400 GeV, and 600 GeV, respectively.

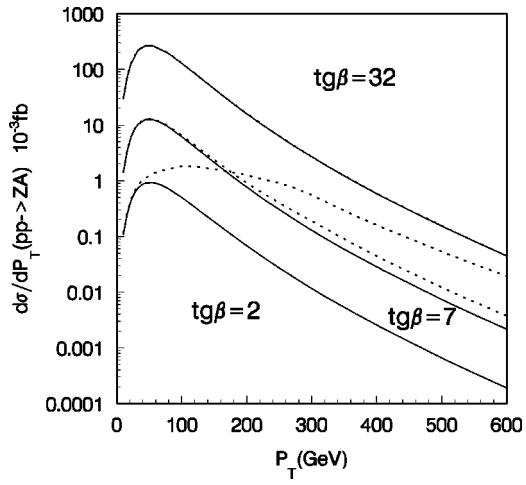

FIG. 9. The differential cross sections $d\sigma^{(DY)}/dp_T$ and $d\sigma^{(T)}/dp_T$ of the process $pp \rightarrow A^0Z^0+X$, as functions of the transverse momentum p_T in the MSUGRA scenario with $\sqrt{s}=14$ TeV, $m_A=350$ GeV, and the pseudorapidity being in the range of $|\eta|<2$. The ratio of the vacuum expectation values $\tan\beta$ is taken as 2, 7, and 32, respectively.

to disentangle the MSSM from the general 2HDM in these parameter space regions.

In Fig. 5, the cross section of the parent process $pp \rightarrow gg \rightarrow A^0Z^0+X$ at the LHC versus $\tan\beta$ is plotted. The values of the neutral CP-odd Higgs boson A^0 mass are set to be 200 GeV, 400 GeV, and 600 GeV, respectively. From the figure, we also find that scalar quark contributions can either enhance or suppress the cross section of the parent process as shown in Fig. 4. Figure 5 together with Fig. 4 shows that when the value of m_A is greater than 400 GeV and $\tan\beta < 8$, the contribution from the scalar quark loop diagrams increases with the decrement of $\tan\beta$. In Fig. 5 the two curves for $m_A=400$ GeV and 600 GeV demonstrate that when $\tan\beta<8$, the scalar quark contribution suppresses the cross section, which means $\sigma_{gg}^{MSSM}<\sigma_{gg}^{2HDM}$, while the scalar quark contribution enhances the cross section when $\tan\beta>20$. These features can be also seen from Fig. 4. The curve for $\tan\beta=2$ in Fig. 4 demonstrates that σ_{gg}^{MSSM} is about two-thirds of σ_{gg}^{2HDM} quantitatively, while the curve for $\tan\beta=32$ shows $\sigma_{gg}^{MSSM}>\sigma_{gg}^{2HDM}$.

Figure 6 displays the differential cross section $d\sigma/dp_T$ of the process $pp \rightarrow gg \rightarrow A^0Z^0$ at the LHC versus transverse momentum p_T with $\sqrt{s}=14$ TeV and the pseudorapidity being in the range of $|\eta|<2$. The A^0 mass is set to be 350 GeV, and $\tan\beta$ is taken as 2, 7, and 32, respectively. We find that for $\tan\beta=2$, the scalar quark contribution suppresses the differential cross section $d\sigma/dp_T$. For $\tan\beta=32$ and $p_T>100$ GeV, the scalar quark contribution enhances the differential cross section. But for $\tan\beta=7$, the scalar quark contribution can either enhance or suppress the differential cross section in different p_T regions.

In Figs. 7, 8, and 9, we plot the the cross sections of the process $pp \rightarrow b\bar{b} \rightarrow A^0Z^0+X$ ($\sigma^{(DY)}$) and the process $pp \rightarrow A^0Z^0+X$ contributions from both Drell-Yan and gluon-gluon fusion subprocesses in the constrained MSSM ($\sigma^{(T)}=\sigma^{(DY)}+\sigma_{gg}^{MSSM}$), as functions of the CP-odd Higgs boson A^0 mass, the ratio of the vacuum expectation values $\tan\beta$, and the transverse momentum p_T, respectively. In these three figures, the solid lines are for the cross sections or differential cross sections of the process $pp \rightarrow b\bar{b} \rightarrow A^0Z^0+X$ via the Drell-Yang subprocess, and the dotted lines are for the process $pp \rightarrow A^0Z^0+X$ via both Drell-Yang and gluon fusion subprocesses. With the comparison between the $\sigma^{(T)}$ (or $d\sigma^{(T)}/dp_T$) and $\sigma^{(DY)}$ (or $d\sigma^{(DY)}/dp_T$), we can know in which parameter space in the constrained MSSM the contribution from the loop mediated subprocess $gg \rightarrow A^0Z^0$ is important.

Figure 7 displays the cross sections of $pp \rightarrow b\bar{b} \rightarrow A^0Z^0+X$ and $pp \rightarrow A^0Z^0+X$ at proton-proton colliders versus the mass of A^0 with $\sqrt{s}=14$ TeV. We choose $\tan\beta=2,7$, and 32, respectively. From Fig. 7, we find that in the region of $\tan\beta \leqslant 7$, the contribution of the gluon-gluon fusion subprocess in the MSSM enhances the cross section, especially, when $\tan\beta=2$, the contribution of the gluon-gluon fusion subprocess is about 80% of the total cross section $\sigma^{(T)}$. In fact, the gluon-gluon fusion subprocess is the most important A^0Z^0 associated production mechanism in this parameter space. From the figure we see also that when $\tan\beta=32$ the difference between $\sigma^{(DY)}$ and $\sigma^{(T)}$ is very small; it means that the contribution of the gluon-gluon fusion subprocess is negligible in this parameter space.

The cross sections of $pp \rightarrow b\bar{b} \rightarrow A^0Z^0+X$ and $pp \rightarrow A^0Z^0+X$ at the LHC as functions of $\tan\beta$ with $\sqrt{s}=14$ TeV are shown in Fig. 8. The mass of the Higgs boson A^0 is taken as 200 GeV, 400 GeV, and 600 GeV, respectively. From this figure we can find also that gluon-gluon fusion subprocess enhances the cross section of the A^0Z^0 associated production at the LHC and will become a very important production mechanism when $\tan\beta<10$. In the region of $\tan\beta>10$, the cross sections of the A^0Z^0 associated production at the LHC are in the range of $1-10^2$ fb. Even the $\sigma^{(T)}$ can reach 300 fb when $\tan\beta=48$ and $m_A=200$ GeV. So the

A^0Z^0 associated production process may be easily observed experimentally if $\tan\beta$ is large enough.

Figure 9 displays the differential cross sections $(d\sigma/dp_T)$ of $pp\to A^0Z^0+X$ and $pp\to b\bar{b}\to A^0Z^0+X$ at the LHC as functions of the transverse momentum p_T with the pseudorapidity being in the range of $|\eta|<2$. We choose $m_A=350$ GeV and take $\tan\beta=2,7$, and 32, respectively. From this figure we can see that at the high p_T region, when $\tan\beta\leqslant 7$, the difference between $d\sigma^{(DY)}/dp_T$ and $d\sigma^{(T)}/dp_T$ is obvious, even when $\tan\beta=2$, the $d\sigma^{(DY)}/dp_T$ can be less than 1% of $d\sigma^{(T)}/dp_T$, which means that the contribution from the $pp\to gg\to A^0Z^0+X$ process is dominant in this parameter space. But when $\tan\beta=32$, the contribution to the total differential cross sections $(d\sigma^{(T)}/dp_T)$ is mainly from the Drell-Yan A^0Z^0 associated production subprocess, and the contribution from the gluon fusion subprocess is negligible.

IV. SUMMARY

In this paper, we studied the neutral CP-odd Higgs boson A^0 production with the association of the Z^0 gauge boson via both Drell-Yan and gluon-gluon fusion subprocesses in the constrained MSSM at the CERN LHC. Numerical analysis of their production rates is carried out with some typical parameter sets in the MSUGRA scenario. Our results show that the cross section in the MSSM is clearly enhanced by the gluon-gluon fusion subprocess in the parameter space with small or moderate $\tan\beta$ values, and we should consider the gluon-gluon fusion subprocess in this parameter space in the calculation of the A^0Z^0 associated production at the LHC. We compared the above results of the process $pp\to gg\to A^0Z^0+X$ in the MSSM with those in the general two-Higgs-doublet model, where the cross section of subprocess $gg\to A^0Z^0+X$ is contributed only by quark loop diagrams. We find that the contributions from the scalar quark loops in the MSSM can either enhance or suppress the cross section obviously and cannot be neglected in some parameter space. The results show also that the A^0Z^0 associated production at the LHC is strongly related to the parameters $\tan\beta$ and the mass of A^0. The total cross section increases with increments of $\tan\beta$ and decreases with increments of m_A.

ACKNOWLEDGMENTS

This work was supported in part by the National Natural Science Foundation of China and a grant from the Education Ministry of China.

[1] S.L. Glashow, Nucl. Phys. **B22**, 579 (1961); S. Weinberg, Phys. Rev. Lett. **1**, 1264 (1967); A. Salam, in *Elementary Particle Theory: Relativistic Group and Analyticity (Nobel Symposium No. 8)*, edited by N. Svartholm (Almquist and Wiksells, Stockholm, 1968), p. 367; H.D. Politzer, Phys. Rep. **14**, 129 (1974).

[2] P.W. Higgs, Phys. Lett. **12**, 132 (1964); **13**, 508 (1964); Phys. Rev. **145**, 1156 (1966); F. Englert and R. Brout, Phys. Rev. Lett. **13**, 321 (1964); G.S. Guralnik, C.R. Hagen, and T.W.B. Kibble, *ibid.* **13**, 585 (1964); T.W.B. Kibble, Phys. Rev. **155**, 1554 (1967).

[3] H.E. Haber and G.L. Kane, Phys. Rep. **117**, 75 (1985).

[4] J.F. Gunion, H.E. Haber, G.L. Kane, and S. Dawson, *The Higgs Hunter's Guide* (Addison-Wesley, Reading, MA, 1990).

[5] H. Nilles, Phys. Rep. **110**, 1 (1984); J. Rosiek, Phys. Rev. D **41**, 3464 (1990); hep-ph/9511250; M. Kuroda, hep-ph/9902340.

[6] J.F. Gunion, H.E. Haber, and C. Kao, Phys. Rev. D **46**, 2907 (1992); M. Spira, Fortschr. Phys. **46**, 203 (1998); M. Spira, A. Djouadi, D. Graudenz, and P.M. Zerwas, Nucl. Phys. **B453**, 17 (1995).

[7] A.A. Barrientos-Bendezu and B.A. Kniehl, Phys. Rev. D **64**, 035006 (2001).

[8] A. Arhrib, M.C. Peyranere, W. Hollik, and G. Moultaka, Nucl. Phys. **B581**, 34 (2000).

[9] S. Kanemura, Eur. Phys. J. C **17**, 473 (2000).

[10] S.H. Zhu, hep-ph/9901221.

[11] Heather E. Logan and Shufang Su, Phys. Rev. D **66**, 035007 (2002).

[12] F. Zhou, W.G. Ma, Y. Jiang, X.Q. Li, and L.H. Wan, Phys. Rev. D **64**, 055005 (2001).

[13] D.A. Dicus, J.L. Hewett, C. Kao, and T.G. Rizzo, Phys. Rev. D **40**, 787 (1989).

[14] A.A. Barrientos Bendezu and B.A. Kniehl, Phys. Rev. D **59**, 015009 (1998).

[15] A.A. Barrientos Bendezu and B.A. Kniehl, Phys. Rev. D **61**, 097701 (2000).

[16] F. Zhou, W.G. Ma, Y. Jiang, L. Han, and L.H. Wan, Phys. Rev. D **63**, 015002 (2000).

[17] O. Brein, W. Hollik, and S. Kanemura, Phys. Rev. D **63**, 095001 (2001).

[18] G.J. Gounaris and P.I. Porfyriadis, Eur. Phys. J. C **18**, 181 (2001).

[19] A.G. Akeroyd, A. Arhrib, and M. Capdequi Peyranere, Mod. Phys. Lett. A **14**, 2093 (1999); **17**, 373(E) (2002).

[20] A.G. Akeroyd, A. Arhrib, and M. Capdequi Peyranere, Phys. Rev. D **64**, 075007 (2001); **65**, 099903(E) (2002).

[21] A.G. Akeroyd, A. Arhrib, and C. Dove, Phys. Rev. D **61**, 071702(R) (2000).

[22] G.J. Gounaris, P.I. Porfyriadis, and F.M. Renard, Eur. Phys. J. C **20**, 659 (2001).

[23] C. Kao, Phys. Rev. D **46**, 4907 (1992).

[24] M. Drees and S.P. Martin, Report No. MAD-PH-879, UM-TH-95-02, hep-ph/9504324.

[25] D.M. Copper, D.R.T. Jones, and P. van Nieuwenhuizen, Nucl. Phys. **B167**, 479 (1980).

[26] Bernd A. Kniehl, Phys. Rep. **240**, 211 (1994).

[27] G. Passarino and M. Veltman, Nucl. Phys. **B160**, 151 (1979).

[28] J. Küblbeck, M. Böhm, and A. Denner, Comput. Phys. Commun. **60**, 165 (1990); T. Hahn, hep-ph/9905354.

[29] Y. Jiang, W.G. Ma, L. Han, Z.H. Yu, and H. Pietschmann, Phys. Rev. D **62**, 035006 (2000).

[30] H.L. Lai, J. Huston, and S. Kuhlmann, Eur. Phys. J. C **12**, 375 (2000).

[31] D.E. Groom *et al.*, Eur. Phys. J. C **15**, 1 (2000); D. Schaile, Report No. CERN-PPE/94-162, 1994.

[32] V. Barger, M.S. Berger, and P. Ohmann, Phys. Rev. D **47**, 1093 (1993); **47**, 2038 (1993); V. Barger, M.S. Berger, P. Ohmann, and R.J.N. Phillips, Phys. Lett. B **314**, 351 (1993); V. Barger, M.S. Berger, and P. Ohmann, Phys. Rev. D **49**, 4908 (1994).

[33] M. Spira, Nucl. Instrum. Methods Phys. Res. A **389**, 357 (1997); A. Djouadi, J. Kalinowski, and M. Spira, Comput. Phys. Commun. **108**, 56 (1998).